

Fusion of Sentinel-1 and Sentinel-2 image time series for permanent and temporary surface water mapping

Filsa Bioresita, Anne Puissant, André Stumpf & Jean-Philippe Malet

To cite this article: Filsa Bioresita, Anne Puissant, André Stumpf & Jean-Philippe Malet (2019): Fusion of Sentinel-1 and Sentinel-2 image time series for permanent and temporary surface water mapping, International Journal of Remote Sensing, DOI: [10.1080/01431161.2019.1624869](https://doi.org/10.1080/01431161.2019.1624869)

To link to this article: <https://doi.org/10.1080/01431161.2019.1624869>



Published online: 09 Jun 2019.



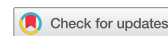
Submit your article to this journal 



Article views: 83



View Crossmark data 



Fusion of Sentinel-1 and Sentinel-2 image time series for permanent and temporary surface water mapping

Filsa Bioresita^{a,b}, Anne Puissant^a, André Stumpf^c and Jean-Philippe Malet^{c,d}

^aLaboratoire Image, Ville, Environnement—LIVE CNRS UMR 7362, Department of Geography, University of Strasbourg, Strasbourg, France; ^bGeodynamic and Environmental Laboratory, Department of Geomatics Engineering, Institut Teknologi Sepuluh Nopember, Surabaya, Indonesia; ^cÉcole et Observatoire des Sciences de la Terre—EOST/CNRS UMS 830, University of Strasbourg, Strasbourg, France; ^dInstitut de Physique du Globe de Strasbourg—IPGS/CNRS UMR 7516, University of Strasbourg, Strasbourg, France

ABSTRACT

Monitoring the spatial and temporal extents of permanent and temporary bodies of surface water is important for various applications such as water resource management, climate modelling, and biodiversity conservation. Satellite remote sensing is an effective source of information to detect surface water over large areas and document their evolution in time. Recently, the European Space Agency (ESA) launched freely available SAR (Synthetic Aperture Radar) and optical sensors (Sentinel-1 & 2) with high revisiting time and spatial resolution. The objective of this paper is to explore the contribution of multi-temporal and multi-source (passive and active) Sentinel observations for improving the detection and mapping of surface waters by applying decision-level image fusion techniques. The approach is tested over Central Ireland using a time series of 16 Sentinel-1 images and a few Sentinel-2 images for the period 2015–2016. Compared to a mono-date approach, the combination of Sentinel-1 & 2 observations provides better accuracy for mapping permanent surface water. Decision level fusion technique allows mapping temporary surface water (such as flooding) with a high accuracy. It also gives the possibility to monitor their dynamics by providing the probability of occurrence of flooded areas at the pixel level.

ARTICLE HISTORY

Received 10 January 2019
Accepted 5 April 2019

1. Introduction

As part of the hydrological system, quantifying the extent of surface water is important in many application fields such as water resource management (with the monitoring of surface reservoirs), climate modelling, biodiversity conservation, food security (such as fishing and crops), and human well-being. Surface water can classically be categorized in two classes: (1) '*Permanent surface water*' and (2) '*Temporary surface water*'. '*Permanent surface water*' is defined as area of the Earth continental surface corresponding to an accumulation of water, showing slight variations in water levels, retaining most of their volumes over the year and that do not dry up. Their variations are mostly dependent on

the hydro-meteorological cycle with rainfall, evaporation and possible overtopping of streams. They can be of natural origin (such as lakes, streams and ponds), or of artificial origin (such as dam reservoirs). The extent and distribution of the permanent surface water are yet poorly and unevenly known at the global scale, since their size varies over several orders of magnitudes, from small ponds to very large lakes often creating inconsistencies in large-scale inventories (Ogashawara, Mishra, and Gitelson 2017). Moreover, mapping permanent surface water is valuable in the context of severe drought response and for water resources management and for hydraulic models validation (Matgen et al. 2010; Pappenberger et al. 2007; Schumann, Di Baldassarre, and Bates 2009).

'Temporary surface water' is defined as waterbody experiencing frequent drying phases (small ponds, puddles and wetlands) or correspond to surfaces frequently affected by flooding, thus causing hazards to human, settlements and infrastructures (Feyisa et al. 2014). Floods can be considered as the most costly type of hazard in terms of property damage and fatalities (Martinis 2010). Since it is impossible to avoid flood risks or prevent their occurrence, flood disaster management is important to reduce their effects. Flood mapping to identify sites in high hazard zones is one of the powerful tools for this purpose (Voigt et al. 2007). Mapping floods will be beneficial to urban and infrastructure planners, risk managers and disaster response, insurance and emergency services during extreme and intense rainfall events.

Today, optical and Synthetic Aperture Radar (SAR) sensors are the most widely used sources to obtain surface water information at continental and local scales. Satellite data provide first order information which is dynamic, near real-time compared with in-situ observation data (Du et al. 2016). Several databases derived from optical or SAR sensors are mapping surface water areas such as the Global Surface Water product of the EC-Joint Research Centre (The European Commission's Joint Research Centre 2016), the SRTM (Shuttle Radar Topography Mission) Water Body product of National Geospatial-Intelligence Agency (Nga 2005), the Global Lakes and Wetlands Database (GLWD) of WWF and the University of Kassel, Germany (WWF 2004), the Water and Wetness product from EC-Copernicus (Copernicus 2015a), and the Landsat Level-3 Dynamic Surface Water Extent (DSWE) Science Product from Earth Resources Observation and Science (EROS) Centre (EROS Center 2018).

The Global Surface Water (GSW) and the DSWE products are generated from Landsat dataset at 30-m spatial resolution. The GSW has a minimum mapping unit of 10 ha. and allows quantifying changes of surface water over a period of 32 years (1984–2015) using expert non-parametric classifiers (Pekel et al. 2016). The SRTM Water Body product is derived from radar data (SRTM Digital Terrain Elevation Data) with a minimum mapping unit of 10 ha. The elevation data are classified based on topographic rules to identify oceans, lakes and rivers (Farr et al. 2007). The Global Lakes and Wetlands Database (GLWD) is generated from various cartographic sources documenting lakes, reservoirs and wetlands on a global scale. The product combines the best existing global and regional maps that were aggregated at a 1-km spatial resolution using expert concepts and thresholds (Lehner and Döll 2004). The product provides a minimum mapping unit of 10 ha. The Water and Wetness product (EC-Copernicus) is produced from Landsat, Sentinel-1, Envisat-ASAR (Advanced Synthetic Aperture Radar) and ancillary GIS (Geographic Information System) datasets. Thresholding is used to derive surface

water from optical and SAR data before fusing the results with GIS datasets to generate the final classification. The minimum mapping unit for this product is 400 m^2 ; the product does not map small river channels and streams of width less than 40 m (Langanke 2016). Two classes of waters are categorized in this product: the ‘permanent water’ class (e.g., rivers and lakes) corresponds to water surfaces identified in, at least, 80% of all observations; the ‘temporary water’ class corresponds to water surfaces identified in more than 25% and less than 80% of all observations.

Consequently, these existing surface water products are relevant for some applications but do not fulfil all the current needs of the science and water management communities. For instance, GLWD and SRTM Water Body do not identify small surface water of less than 10 ha and narrow waterbodies such as watercourses or streams. GSW and DSWE are based on Landsat imagery with gaps in the observation records because of the occurrence of clouds. The Water and Wetness product is using Sentinel-1 data but relies on 30 m spatial resolution Landsat imagery. Figure 1 presents an overview of the existing products for the case study in Ireland.

Nowadays, there has been significant progress in SAR-based mapping of surface water (Martinis 2017). Microwave SAR sensors can penetrate clouds, therefore offer

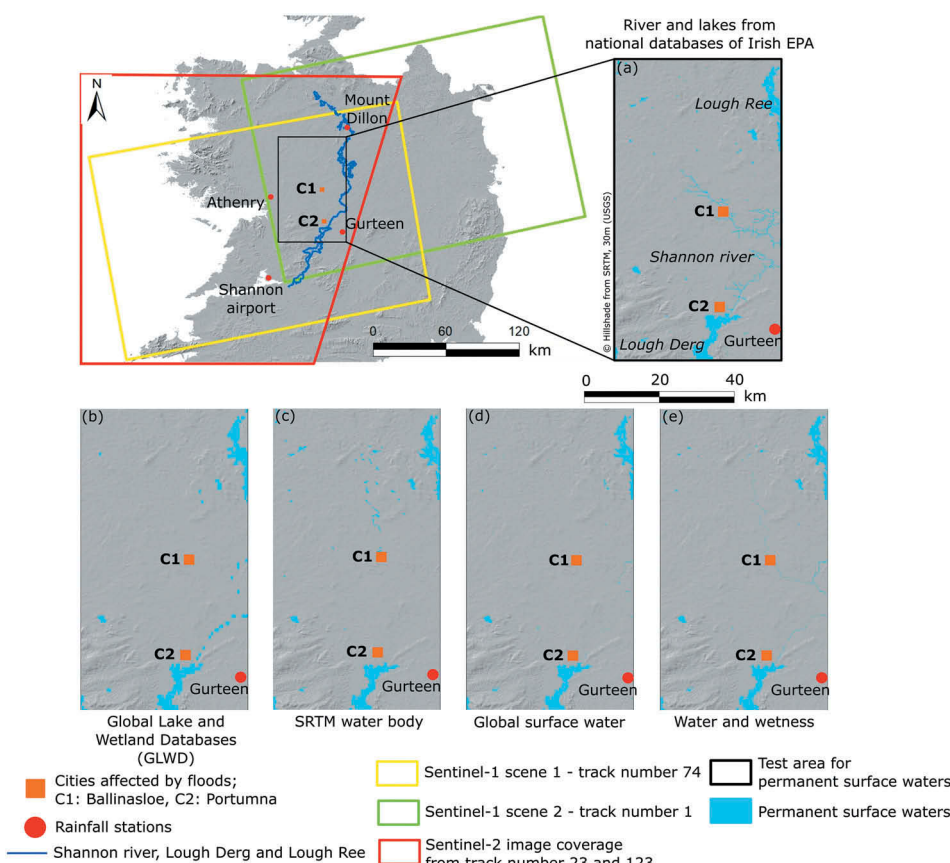


Figure 1. Coverage of datasets and study area with subset of existing product on permanent surface water mapping.

more benefits to observe surface water (and more specifically floods) than optical sensors. The increased availability of SAR images at high spatial and temporal resolution over large areas (Martinis 2010; Martinis and Twele 2010; Pierdicca et al. 2013) and the development of automatic algorithms to extract surface water (Bioresita et al. 2018; Clement, Kilsby, and Moore 2017; Martinis and Twele 2010; Twele et al. 2016) add value to this source of information (Martinis 2017; Martinis and Twele 2010).

The most common method used to discriminate water and non-water areas in SAR images is thresholding (Bartsch et al. 2012; Martinis, Twele, and Voigt 2009; Muster et al. 2013). These methods are based on the contrast of low backscattering values over waterbodies and high backscattering values over the surrounding terrains. The accuracy of the detection algorithms varies depending on the land cover classes observed in the scene and of the topography. For example, in urban areas, water detection is very challenging due to the shadowing effects from buildings as a result of the side-looking viewing geometry of SAR satellite sensors. Further, waters beneath vegetation layers are difficult to detect due to double bounce scattering resulting in a drastic increase of radar backscatter (Martinis 2010). The presence of strong wind that roughens the water surfaces can also produce misclassification errors. Flat areas also can give low backscattering values which can generate misinterpretation as water surfaces. A method for automatic and rapid mapping of water surfaces has been presented in (Bioresita et al. 2018). The method uses finite mixture models and bilateral filtering as a smooth labelling for defining the thresholds. This approach was applied to three sites recently affected by flooding events using mono-date Sentinel-1 data. The method gives successful results in terms of water surfaces (and in all subsequent cases) detection as it relies on significant contrast of pixel values between water and non-water areas. However, the method gives misclassification if non-water areas have lower backscattering values than water areas such as airport runways or some agricultural fields where specular reflection is observed.

Optical data provide information on the multispectral reflectivity of surface water whereas SAR data provide information on the texture (Chaouch et al. 2012; Markert et al. 2018) of the surface water. Optical images such as Landsat, SPOT (Satellite Pour l'Observation de la Terre) and IKONOS have been used for surface water mapping in several studies (Marcus and Fonstad 2008; Nath and Deb 2010; Ogilvie et al. 2018). For instance, Martinis (2017) and Ogilvie et al. (2018) proved the capability of Landsat and Sentinel-2 data for mapping small waterbodies of about 1 to 10 ha. The most widely used methods for surface water detection in optical imagery are based on water indices (Feyisa et al. 2014; Rokni et al. 2014; Wang, Huang, and Wei 2013). Indices combine spectral bands using various algebraic operations to increase the difference between waterbodies and land. Limitations in the detection are however caused by the quality of the water body types in terms of colour (Jiang et al. 2014).

In 2014, the European Space Agency (ESA) launched the Sentinel constellation including free available SAR and optical data (Sentinel-1 & 2) with high revisiting time (5 to 12 days) and high spatial resolution (10 to 30 m). This constellation offers the possibility to increase the capture of genuine time series. The combination of remote sensing data with different characteristics is a standard remote sensing problem that has been extensively investigated in the literature (Chavez 1991). The main aim consists in fusing multi-sensor information as a means of combining the respective advantages of

each sensor (Goyal and Wahla 2015). Combining existing sensors can mitigate limitations of any one particular sensor for various land cover issues (Gamba 2014; Joshi et al. 2016). Complementary observations can thus be exploited for land cover mapping purposes. More specifically, many case studies present methods for surface water extraction based on multi-source (optic and SAR) image fusion. Fusion of heterogeneous image source has been widely investigated in the remote sensing (Benediktsson et al., 2018; Chavez 1991; Schmitt and Zhu 2016). Image fusion can be implemented at three different levels (Ghassemian 2016; Liu et al. 2018): (1) pixel level, (2) feature level and (3) decision level. The decision level approach is commonly used for surface water extraction. When images originate from several sensors, the most relevant method for data fusion is to combine the images with the surface waters results extracted individually for each image source (Chengquan et al. 2018; DeVries et al. 2017; Huang et al. 2018; Pohl and Van Genderen 1998; Wendl et al. 2018; Westerhoff et al. 2013).

In conclusion, using image time series and data fusion techniques to increase the accuracy of permanent surface waters detection is promising (Bourgeau-Chavez et al. 2009; Liu et al. 2018; Riffler et al. 2018). Combining data of different properties and acquired at several periods can improve image classification (Riffler et al. 2018). However, even though promising, there are only a few studies combining multi-temporal and multi-source approach. In this context, the hypothesis is that SAR and optical satellite time series (Sentinel-1 & 2) are relevant to fill the gap for producing permanent and temporary surface water maps. The objective of our work is to investigate and quantify the performance of Sentinel-1 and Sentinel-2 time series for improving surface water mapping by applying decision-level fusion techniques. The approach is being tested on image time series over Central Ireland ([Figure 1](#)) for the period 2015–2016.

2. Study area and datasets

The use case is the catchment of the Shannon River in Central Ireland. This area is of specific interest in developing and testing the methodology as (1) the density of permanent surface water (e.g., lakes and rivers) is high, (2) the variation in spatial extents over the season is moderated because of the oceanic temperate climate, and because (3) the catchment was affected by severe flooding events in Winter 2015/2016 altering the spatial extent of water surfaces for some days (McCarthy et al. 2016). Further, the weather conditions over Ireland, with only 20% of time (per year) with cloud-free Sentinel-2 optical data, justify the use of Sentinel-1 SAR data to document the water surfaces. [Figure 1](#) presents the study area of size ($\pm 3657 \text{ km}^2$) as well as the permanent surface water documented, respectively, in the global databases GSW, GLWD, SRTM Water Body, Water & Wetness and in the national database of the Irish Environmental Protection Agency (Epa 2017).

Over the study area, the extent of the water surfaces can omit of $\pm 92 \text{ km}^2$ in GSW, $\pm 120 \text{ km}^2$ in GLWD, $\pm 114 \text{ km}^2$ in SRTM Water Body, $\pm 99 \text{ km}^2$ in Water & Wetness, and $\pm 111 \text{ km}^2$ in the national EPA database. The permanent surface water has been severely altered by a series of extratropical cyclones occurring from the end of 2015 to the beginning of 2016 causing flooding between Ballinasloe and Portumna ([Figure 1](#); C1 and C2). Storm Desmond took place on 4 December 2015. During the storm, Keenagh Beg rain gauge station in Co Mayo, recorded the highest daily rainfall since 1944, with a 24 h total of

Table 1. Catalogue of images used for the analysis.

Sentinel-1 acquisition	Track number	Orbit	Time series	Information	Sentinel-2 acquisition *image cloud free	Track number	Cloud cover (%)
22 November 2015	74	Ascending	t1	Dry	/	/	/
16 December 2015	74	Ascending	t2	Flooding	22 December 2015	23	5.6
28 December 2015	74	Ascending	t3				
9 January 2016	74	Ascending	t4	Flooding	/	/	/
14 February 2016	74	Ascending	t5	Dry	/	//	/
26 February 2016	74	Ascending	t6	Dry			
9 March 2016	74	Ascending	t7	Dry	/	/	/
21 March 2016	74	Ascending	t8	Dry			
14 April 2016	74	Ascending	t9	Dry	/	/	/
8 May 2016	74	Ascending	t10	Dry	/	/	/
8 June 2016	1	Ascending	t11	Dry	/	/	/
14 July 2016	1	Ascending	t12	Dry	18 July 2016	23	6.6
19 August 2016	1	Ascending	t13	Dry	/	/	/
12 September 2016	1	Ascending	t14	Dry	/	/	/
18 October 2016	1	Ascending	t15	Dry	/	/	/
30 October 2016	1	Ascending	t16	Dry			
					6 November 2016	23	4.5

161 mm (Éireann 2015). Road networks, grasslands and croplands were submerged during flooding period (National Directorate for Fire and Emergency Management 2016).

A time series of 16 Sentinel-1 images in IW GRDH (Ground Range Detected in High resolution) mode and covering the period between 22 November 2015 to 30 October 2016 is used. The time series includes two images where flooding is observed. The images have a spatial resolution of 20 m × 22 m with double polarization (VV and VH). The images cover the study area with two orbit tracks (scene 1-track number 74; scene 2-track number 1) in ascending mode. Three cloud-free (cloud coverage < 15%) Sentinel-2 images (level 1C) are used as complementary source of information (Table 1).

Topographic information from the SRTM 1 Arc-Second Global at 30-m spatial resolution is used in order to construct topographic index maps (HAND; Height above Nearest Drainage; Rennó et al. 2008) for the Sentinel-1 data analysis. Further, rainfall data from the rain gauges located at Shannon airport, Gurteen, Athenry, and Mount Dillon are used for the analysis of temporary surface water (Éireann 2016).

3. Methodology

The general methodology is described in Figure 2. The detection of the surface water and the calculation on the probability of occurrence are carried out on the Sentinel-1 images with the Water-S1 method presented in (Bioresita et al. 2018). An adaptation of the Water-S1 method is used for the processing of the optical Sentinel-2 data (see Section 3.1). The occurrence maps obtained for the two time series (Sentinel-1, Sentinel-2) are combined using decision level methods (see Section 3.2). Finally, the fused results are evaluated for the permanent surface waterbodies and for the temporary flooded areas for the corresponding time periods (see Section 3.3).

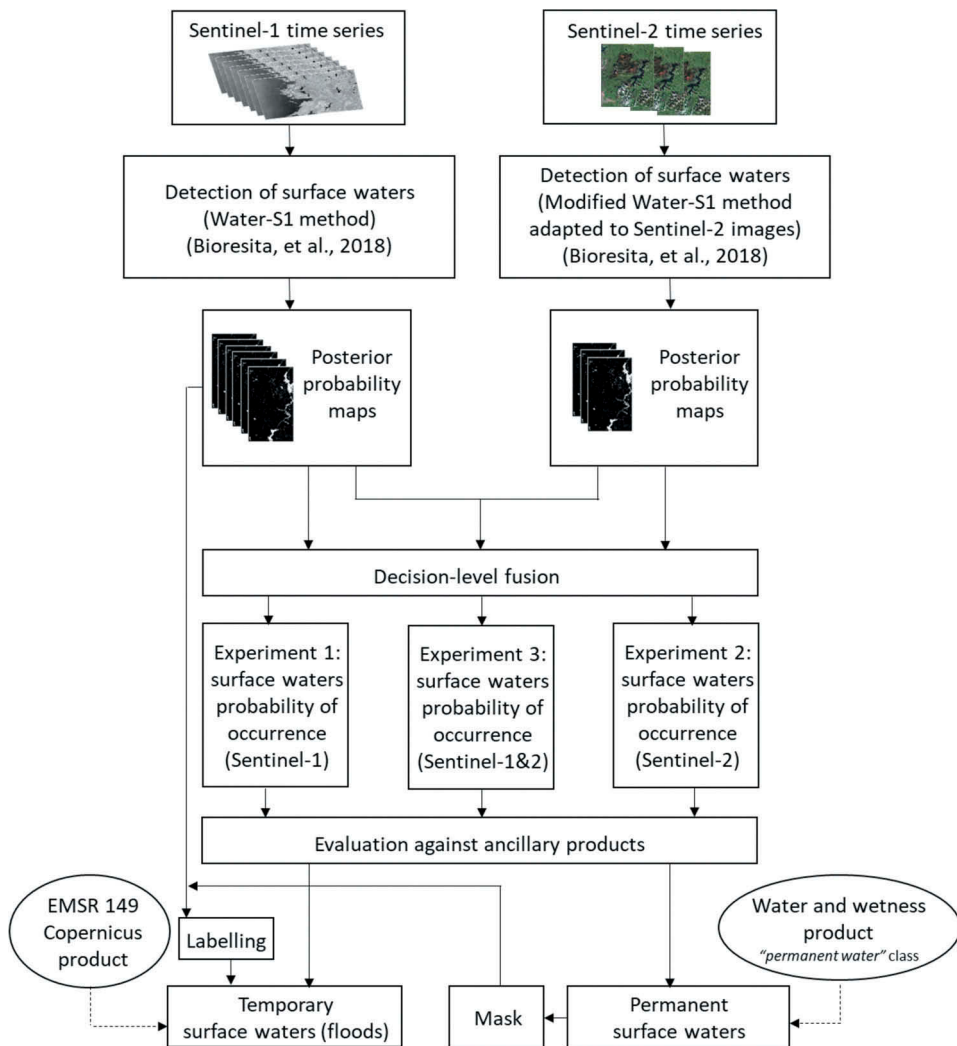


Figure 2. Methodological workflow.

3.1. Extraction of surface water and calculation of probability of occurrence maps from sentinel-1 and sentinel-2 images

The processing of Sentinel-1 IW GRDH image is based on the Water-S1 method described in (Bioresita et al. 2018) and summarized in Figure 3. The first step consists of a correction of orbital errors, speckle noise and geometric distortion of the data. The application of precise Sentinel orbits, the radiometric calibration of the SAR images to Sigma-nought images, the multi-looking, the filtering of speckle, and terrain relief is applied in the Sentinel Application Platform/SNAP (Foumelis 2015; Stewart 2016). Then, a subset of Sigma-nought images is masked using the Height above Nearest Drainage (HAND) terrain index. This index is based on the drainage network and is used to constrain the processing area in order to avoid classification errors in topographically non-plausible water areas. A threshold of $\text{HAND} < 15 \text{ m}$ is applied in order to filter the

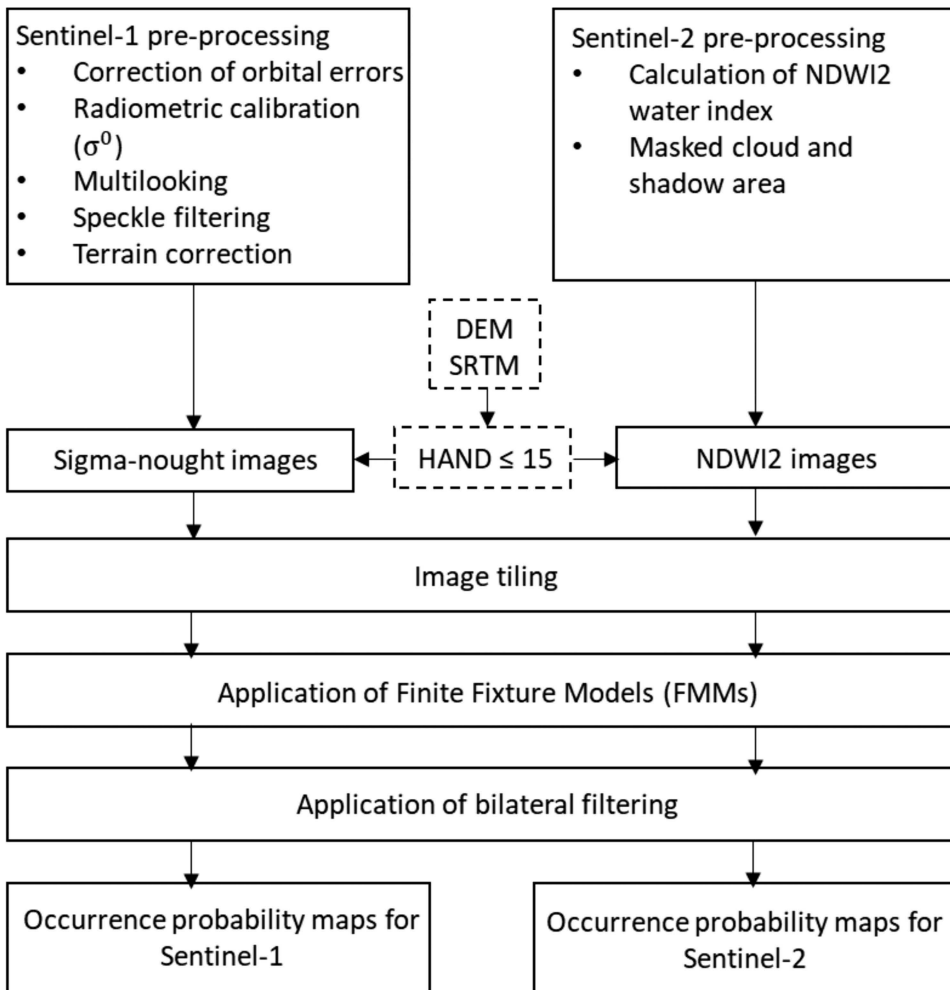


Figure 3. Flowchart of surface water extraction: Water-S1 method (for Sentinel-1) and modified Water-S1 method applied to Sentinel-2 mono-date images.

false positives of surface water located above the nearest drainage line. Then, a statistical modified Split-Based Approach (SBA) is used in order to tile the input images into squared non-overlapping blocks of 10×10 km size and to select the tiles for class modelling. The strategy for tile selection consists of choosing only the image tile which contains some portions of surface water based on Hartigan's dip statistic (HDS) value (Freeman and Dale 2013). Class modelling is performed by applying Finite Mixture Models (FMM) (Benaglia et al. 2009). The model parameters for each tile are calculated, then global sets of parameters are defined and probabilities of occurrences are computed. Finally, a labelling using Bilateral Filtering is applied to the occurrence images (Schindler 2012). The filtered occurrence probability images are then used as input data for image fusion.

For Sentinel-2, the general workflow of Water-S1 is applied with some adaptations. First, the Sentinel-2 level 1C (Top of Atmosphere values) are corrected to level 2A

(Bottom of Atmosphere values) using Sen2Cor (Louis et al. 2016), and cloud and shadow area are masked. The NDWI2 water index (Equation (1)), classically used to extract water surfaces (Martinis 2017; McFeeters 1996), is calculated at 10-m spatial resolution and is used for feature extraction.

$$NDWI2 = \frac{(R_{Band3} - R_{Band8})}{(R_{Band3} + R_{Band8})} \quad (1)$$

where R represents the reflectance value of the band. Band3 is the green band and Band8 is the near-infrared band.

The HAND topographic index (Rennó et al. 2008) is calculated on the SRTM topography and applied to the NDWI2 images in order to remove regions located above the nearest drainage line and avoid misclassification.

3.2. Methods of image fusion: decision-level fusion rules

Image fusion can be implemented at three different levels: (a) pixel, (b) feature, or (c) decision level (Liu et al. 2018). When images originate from several sensors, the most relevant method for data fusion is to combine the images with the surface water results extracted individually for each image source (Pohl and Van Genderen 1998; Wendl et al. 2018; Zadeh 1976).

Several methods of decision level fusion are compared in order to identify the most suitable approach for surface water. This information is fused in order to create value-added layers (Zadeh 1976). Probabilities of occurrence of surface water are calculated, first, in order to evaluate the interest of time series to enhance the mapping and, second, to evaluate the complementarity of results from the SAR and optical sensors. All calculations are performed at pixel level by combining the probabilities of occurrence of each experiment (experiment 1 = time series of Sentinel-1 data, experiment 2 = time series of Sentinel-2 data, experiment 3 = time series of Sentinel-1 and Sentinel-2 data). The final image fusion is expressed in terms of posterior probability.

The fuzzy logic method and the Bayesian method are tested for the decision level fusion. The most powerful fusion method identified for Sentinel-1 results is then applied for the fusion of the Sentinel-2 results and for the fusion of Sentinel-1 and Sentinel-2 results (see Section 4.1.1).

Image fusion using fuzzy logic (Wendl et al. 2018) is powerful to combine uncertain data. Considering a reference set L of classes, then a fuzzy set A in L , is a set of ordered pairs:

$$A = [(x, P_A(x) | x \in L)] \quad (2)$$

where $P_A : L \rightarrow [0, 1]$ is the membership function of A in L which range is a subset of the nonnegative real numbers whose supremum is finite. The algorithm proposed by (Wendl et al. 2018) is used for the calculation. It uses a minimum number of fuzzy logic operators (Equation (3)). The details of the membership functions are presented in Figure 4. The fuzzy logic minimum operator is used based on the accurate results obtained by Wendl et al. (2018) for urban land use classification.

$$P_{fusion}(x) = \text{Min} (P_A(x), P_B(x)) \quad (3)$$

Degree of membership

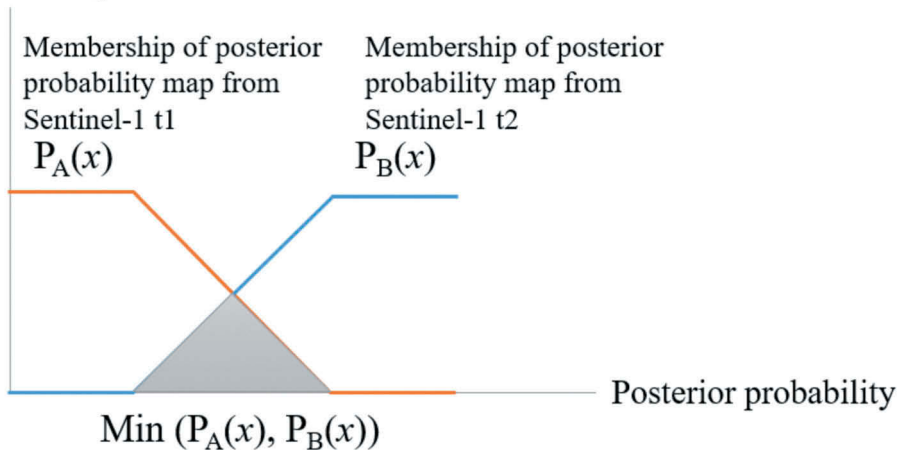


Figure 4. Decision-level fusion: Application of the fuzzy logic minimum operator, with an example of combination of Sentinel-1 posterior probability maps (t1 and t2, see Table 1).

The second approach for data fusion is Bayesian, with algorithm proposed by Wendl et al. (2018). Bayesian approach is also used based on the accurate results obtained by Wendl et al. (2018) for urban land use classification. It executes image fusion based on the operator product (Equation (4)) or operator sum (Equation (5)).

$$P_{\text{fusion}}(x) = P_A(x) \times P_B(x) \quad (4)$$

$$P_{\text{fusion}}(x) = P_A(x) + P_B(x) \quad (5)$$

where P_A and P_B are the posterior probability maps.

3.3. Evaluation procedure

A threshold of 90% is used to differentiate the '*permanent surface water*' (posterior probability > 90%) from other classes (posterior probability < 90%). The '*permanent water*' class of the Water and Wetness product is used as the reference product for the evaluation of the '*permanent surface water*' detected with our methodology. The reasons are that the Water and Wetness product is produced from Sentinel-1 (Figure 1 – Subset (e); see Section 1), and has nearly the same spatial resolution as our results.

The '*temporary surface water*' in our study was extracted from Sentinel-1 images using the '*permanent surface water*' map issued from the best fusion algorithm and the best experiment as a mask. Due to the flooding events of December 2015 and January 2016, the '*temporary water*' class of the Water and Wetness product cannot be used as reference data. Therefore, for the evaluation of the '*temporary surface water*' detected with our methodology, the Copernicus Emergency Management Service (EMS) (Copernicus 2015b) maps are used. For the period of interest, only one EMS product is available (9 January 2016) to assess flooding event on that date.

All the quantitative assessments are based on the calculation of confusion matrices and of indicators such as the Overall accuracy, the *F*-measure, the True Positive Rate (TPR), the False Positive Rate, and the Omission and Commission error. Qualitative assessment is also applied and presented in [Section 4](#) for the permanent surface water (see [Section 4.1](#)) and the temporary surface water (see [Section 4.2](#)).

4. Results

4.1. Mapping of ‘permanent surface water’

4.1.1. Mono-date detection of surface water from sentinel-1 and sentinel-2 images

[Figure 5](#) presents the detection of water surfaces over the region of Portumna ([Figure 1, C2](#)) for the 16 Sentinel-1 images and the 3 Sentinel-2 images expressed in terms of occurrence probability maps. The maps are binarized in two classes (presence and absence of water) using a posterior probability threshold >90% (Bioresita et al. 2018). The surface extents vary in the range 86 to 225 km² over the period. In the Sentinel-1 time series, during the flooding period of Winter 2015/2016, water is detected in the North area of Lough Derg until 14 February 2016. Extraction of water surfaces in April, June and October 2016 presents some errors due to roughness of the water surfaces caused by wind and turbulence effects. Roughness causes a higher backscattering signal and therefore an enhanced brightness in the SAR data. In the Sentinel-2 image of December 2015, surface water is clearly depicted in the north area of Lough Derg. Due to the presence of thin cirrus and dark pixels areas, surface water areas are overestimated for the Sentinel-2 image of November 2016. In order to overcome those problems, decision-level fusion is performed.

4.1.2. Multi-date detection of “permanent surface water” with time series image fusion

Results of image fusion of the Sentinel-1 time series images are presented in [Figure 6](#). All fusion results present a reduction in the noise level. However, comparison with the reference product indicates different performances of the decision-level rules. Test 1 (operator fuzzy logic Min) only identifies fractions of Lough Derg and is not able to identify the permanent surface water along Shannon River; test 2 (Bayesian operator product) does not identify Lough Derg and the Shannon River (presence of false negative); test 3 (Bayesian operator Sum) gives the best results with the identification of the Shannon River and of nearly the full area of Lough Derg.

The quantitative assessment ([Table 2](#)) indicates high overall accuracies of above 99%. Test 2 gives very low *F*-measure with a value of about 0.55 and True Positive Rate (TPR) with a value of about 38%. Omission error of Test 2 is very high reaching 61%. Test 1 gives better *F*-measure than Test 2 with a value of 0.77, but the TPR is low with a value of 62%. Omission error in Test 1 is also high with a value of 37%. Those measures explain the appearance of a large amount of false negatives ([Figure 6](#)) for Test 1 and Test 2 even if the overall accuracies are high. Test 3 shows the highest overall accuracy and *F*-measure with a value of 0.99, a high TPR with a value of 98% and low omission error with a value of 1.4%. As a consequence, the Bayesian sum operator is used and

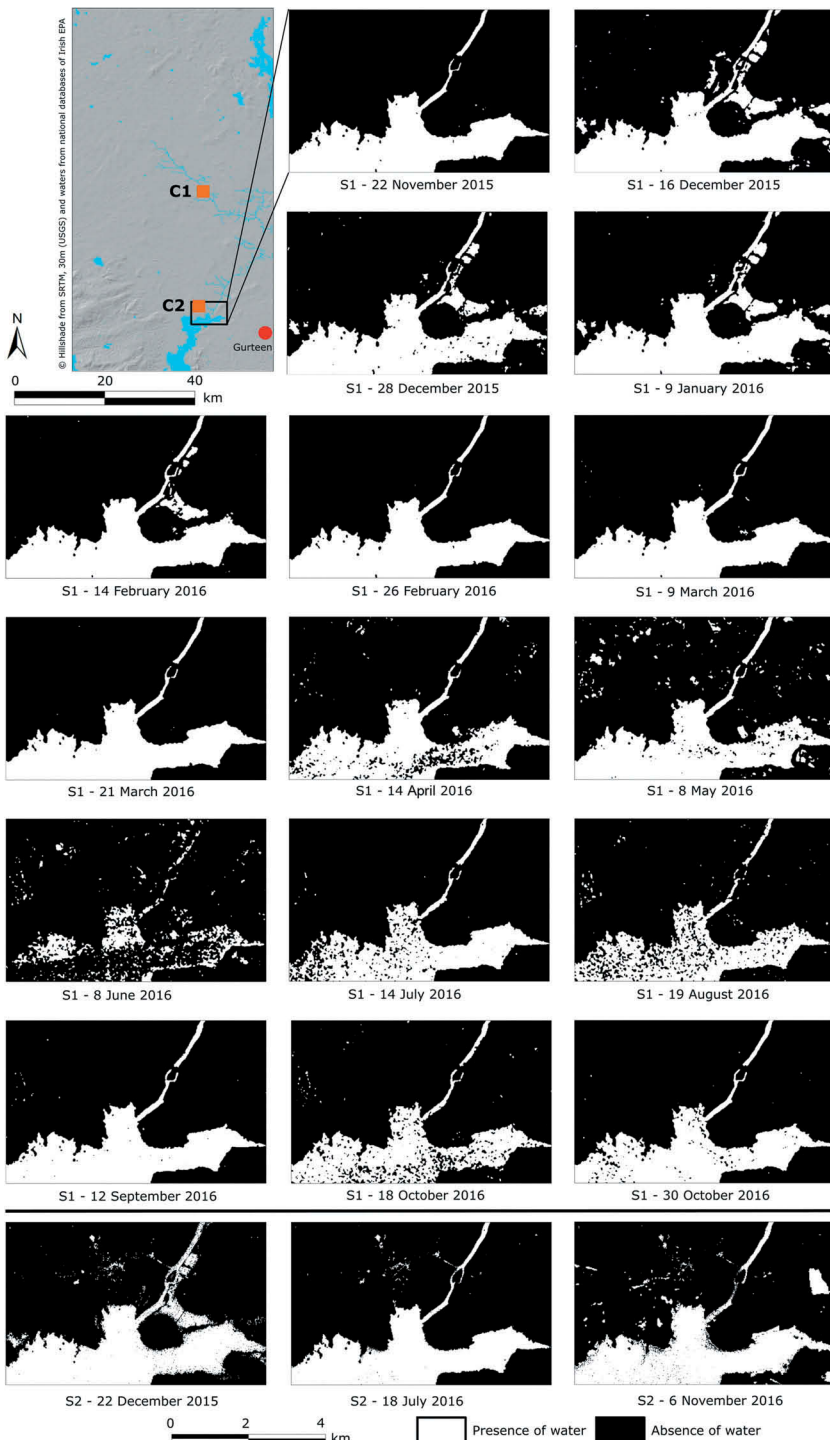


Figure 5. Surface water detected for the 16 Sentinel-1 images and the 3 Sentinel-2 images in terms of occurrence probability maps, with a zoom on the region of Portumna (C2).

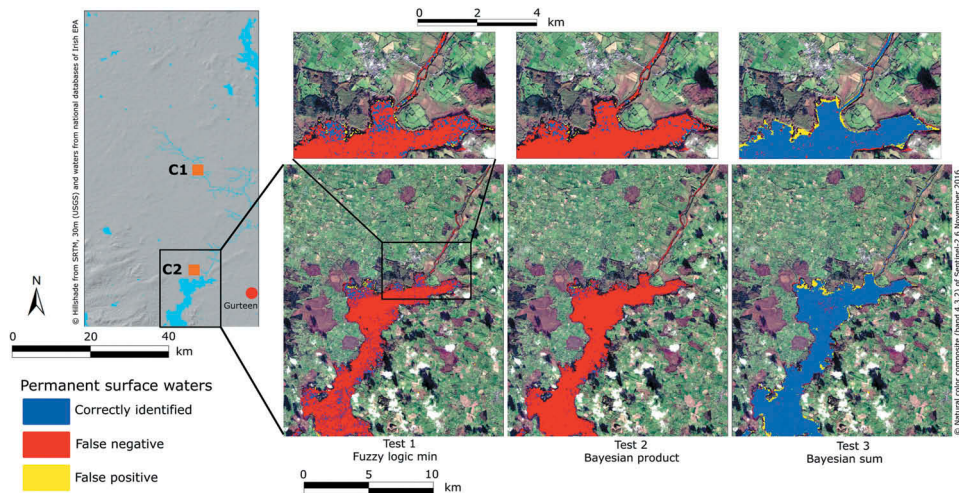


Figure 6. Decision-level fusion results for the Sentinel-1 time series over the region of Portumna, with details (zoom) on the north bank of Lough Derg and for the three methods of image fusion.

Table 2. Classification accuracy of Sentinel-1 time series for the three methods of decision-level fusion.

Test	Method	Overall accuracy (%)	F-measure	True positive rate (%)	False positive rate (%)	Omission error (%)	Commission error (%)
Test 1	Fuzzy min	99.50	0.77	62.473	0.002	37.52	0.30
Test 2	Bayesian Product	99.32	0.55	38.301	0.001	61.69	0.26
Test 3	Bayesian Sum	99.94	0.99	98.602	0.023	1.39	0.83

applied for the fusion of the multi-temporal Sentinel-2 images (experiment 2), and for the fusion of Sentinel-1 and Sentinel-2 time series (experiment 3).

Table 3 summarizes the comparison of the three experiments of image fusion to the Water & Wetness products considered as reference data. Results of decision-level fusion from Sentinel-2 images (Experiment 2) are presented in Figure 7. Experiment 2 gives the best TPR and omission error than the other experiments, but it is based only on three images with a low cloud density. Experiment 2 allows detecting both the Lough Derg and the Shannon River at high accuracy with an overall accuracy of 99%, an F-measure of 0.99 and a TPR of 99%.

Table 3. Comparison of image fusion results with the water & wetness reference data.

Experiment (with Bayesian operator sum)	Overall accuracy (%)	F-measure	True positive rate (%)	False positive rate (%)	Omission error (%)	Commission error (%)
Experiment 1 (S1)	99.94	0.98	98.60	0.02	1.40	0.83
Experiment 2 (S2)	99.95	0.98	99.20	0.04	0.80	1.79
Experiment 3 (S1 & S2)	99.95	0.99	98.31	0.01	1.69	0.34

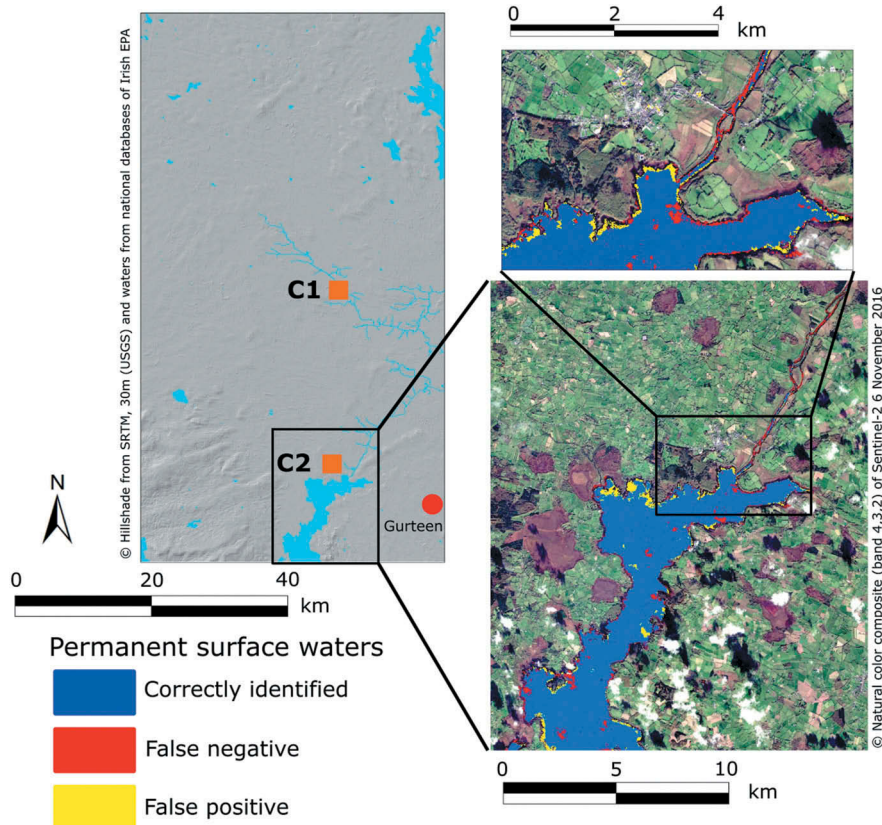


Figure 7. Decision-level fusion results for the Sentinel-2 images over the region of Portumna, with details (zoom) on the north bank of Lough Derg.

Results of decision-level fusion from Sentinel-1 and Sentinel-2 time series (Experiment 3) are presented in Figure 8. Experiment 3 gives better values in terms of overall accuracy (>99%), *F*-measure (0.99), and TPR (98%) than the other experiments. The omission error is very low (1.7%). A few false negatives are observed mainly along the borders of the surface waterbodies (Figure 8; sectors a, b, c). False positives are detected on the borders of Lough Derg (Figure 8; sector d). In all experiments, the surface water is detected at very high accuracy with an overall accuracy of more than 99%, an *F*-measure of 0.99, and a TPR more than 98%.

Considering all the parameters using for accuracy assessment, the best result is obtained with the fusion of Sentinel-1 and Sentinel-2 time series with the Bayesian operator sum.

4.2. Mapping of ‘temporary surface water’: flooded areas

‘Temporary surface water’ bodies are extracted for the Sentinel-1 image of 09/01/2016 by applying the ‘permanent surface water’ map calculated from experiment 3 (S1&S2) with Bayesian sum operator as a mask. Table 4 indicates high overall accuracy (>98%),

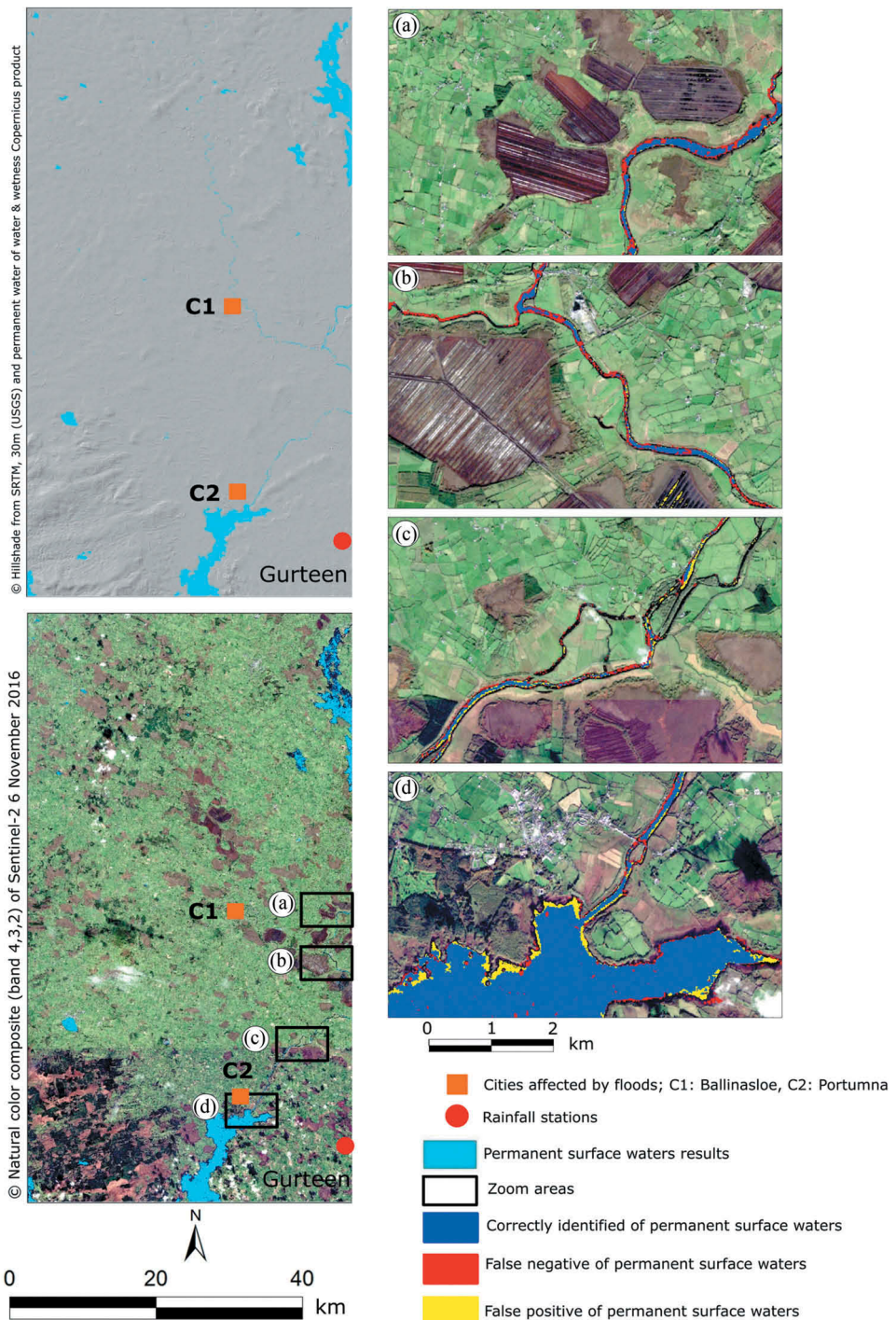


Figure 8. Decision-level fusion results for the Sentinel-1 and Sentinel-2 images over the region of Portumna, with details (zoom) on the Shannon River (sector a, b, c) and the north bank of Lough Derg (sector d).

Table 4. Comparison of image fusion results with the flood map of EMS Copernicus used as reference data for the date 9 January 2016.

Date	Overall accuracy (%)	F-measure	True positive rate (%)	False positive rate (%)	Omission error (%)	Commission error (%)
9 January 2016	98.79	0.90	86.07	0.35	13.92	5.72

F-measure (0.90) and TPR (86%) for the detection of these '*temporary surface water*' bodies; the omission error is low (13.9%).

Figure 9 identifies false positives along the borders of the Lough Derg Lake and along the Shannon River. These false positives are related to sandbank in the course of the river or to narrow river banks identified as '*temporary surface water*' in our results while they are identified as '*permanent surface water*' in the flood map of the Copernicus Emergency Management Service (EMSR149). The image fusion method allows mapping almost all flooded areas as proven by the little amount of false negatives (Figure 9).

5. Discussion

Surface water dynamics can be monitored from the detection of '*temporary surface water*' from the time series images. These surfaces are extracted by applying the '*permanent surface water*' (detected in experiment 3) as a mask to posterior probability of Sentinel-1 time series. The remaining surfaces correspond to '*temporary surface water*' bodies (ca. 900 km² over the study area). These areas are presented in a frequency map (Figure 10(a)) which mapping the number of times a pixel is classified in '*temporary surface water*' bodies over the study area and for the complete time series. These areas are close to the main streams and located in the most flat areas of the region (Figure 10 (a)). The pixels only classified once as '*temporary surface water*' bodies represent nearly 49% of the surfaces and can be excluded from '*temporary surface water*' bodies as they can be considered as noise or misclassification. The pixels with a frequency higher than 9 correspond to areas spatially close to the '*permanent surface water*' bodies and represent about 3% of the surfaces. Therefore, the pixels classified at least 2 times and less than 9 times (Figure 10(b)) are considered as the final '*temporary surface water*' maps.

It is further possible to relate the detected '*temporary surface water*' bodies to the annual rainfall amounts. In December 2015, the largest amount of '*temporary surface water*' bodies are observed over the one-year period (Figure 11) in relation to Storm Desmond (Jiang et al. 2014). In January 2016, for lower amount of monthly rainfall, flooded areas are still observed because the water did not infiltrate in the soil or was evacuated by the drainage network. In Spring and Summer 2016, the surfaces of '*temporary surface water*' bodies decrease in relation to the decrease in rainfall. In May and June 2016, the detected waterbodies seems to be overestimated probably because of higher noise in the Sentinel-1 images caused by strong wind and rough water surfaces. In Autumn 2016, only small surfaces of '*temporary surface water*' bodies are detected; the precipitation events of September 2016 did not cause flooding.

The spatiotemporal dynamics of the '*temporary surface water*' bodies is further analysed for the period November 2015 to April 2016 by interpreting the frequency value 2 to 4 (Figure 12). The histogram of the possible pairwise combination (frequency

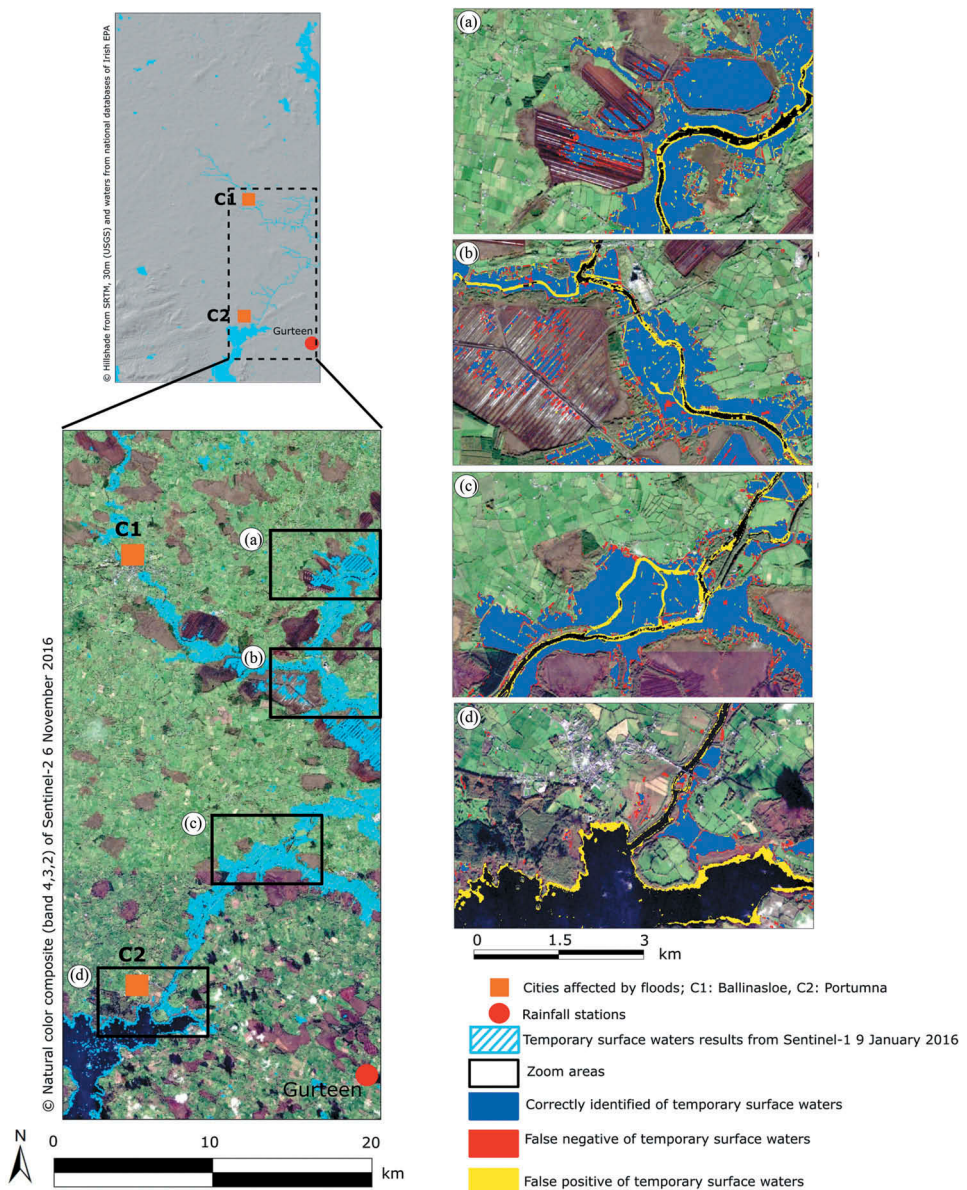


Figure 9. Detection of the ‘temporary surface water’ bodies in the Sentinel-1 image of 9 January 2016 and comparison to the flood map of Copernicus EMS, with details (zoom) on the Shannon River (sector a, b, c) and the north bank of Lough Derg (sector d).

2) indicates that the maximum surfaces of flooded areas are observed for the period t₂-t₃ and t₃-t₄ (Figure 12(a)); these flooded areas correspond spatially to local agricultural lands flooded during less than 4 weeks. The histogram of the possible combination of frequency 3 indicates that the maximum surfaces of flooded areas are observed for the period t₂-t₃-t₄ (Figure 12(b)); these flooded areas correspond spatially to larger agricultural lands flooded during less than 6 weeks. Finally, the histogram of the possible

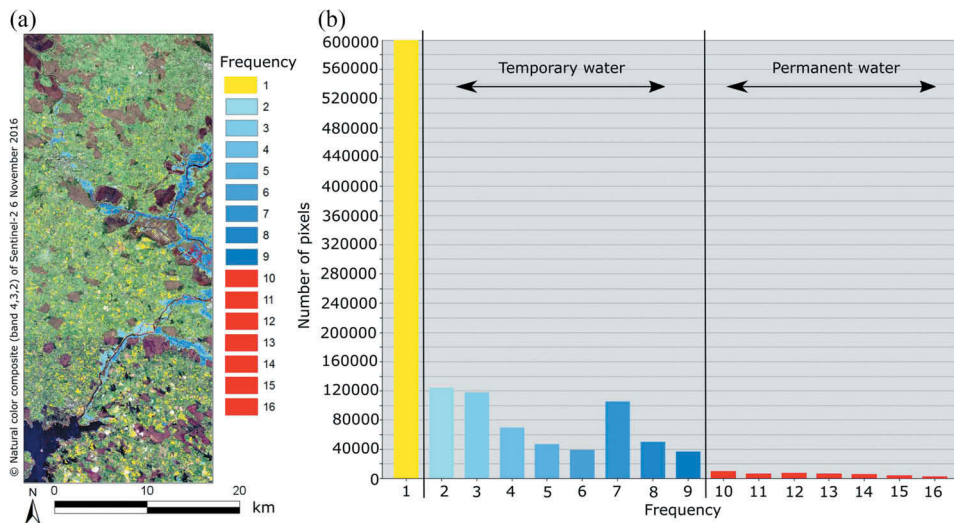


Figure 10. Frequency map and histogram of ‘temporary surface water’ bodies detected in the Sentinel-1 time series (16 images).

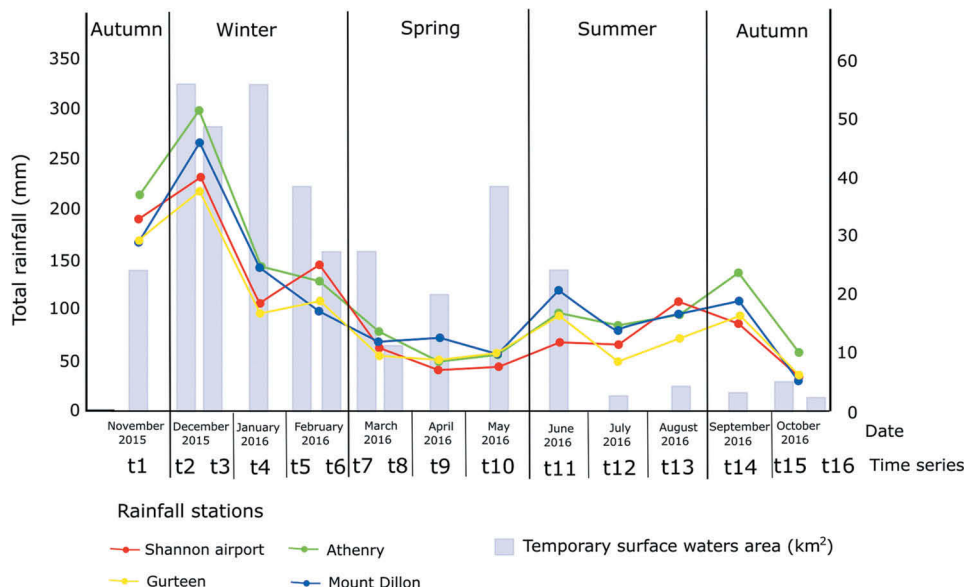


Figure 11. Distribution of ‘temporary surface water’ bodies per period and relation to the monthly rainfall amount for one hydrological year (November 2015 – October 2016).

combination of frequency 4 indicates that the maximum surfaces of flooded areas are observed for the period t2-t3-t4-t5 (Figure 12(c)); these flooded areas correspond spatially to agricultural lands and wetlands flooded during more than 8 weeks.

The results show high similarity of permanent surface water with the Water & Wetness product using other fusion methods. In this study, the methodology was

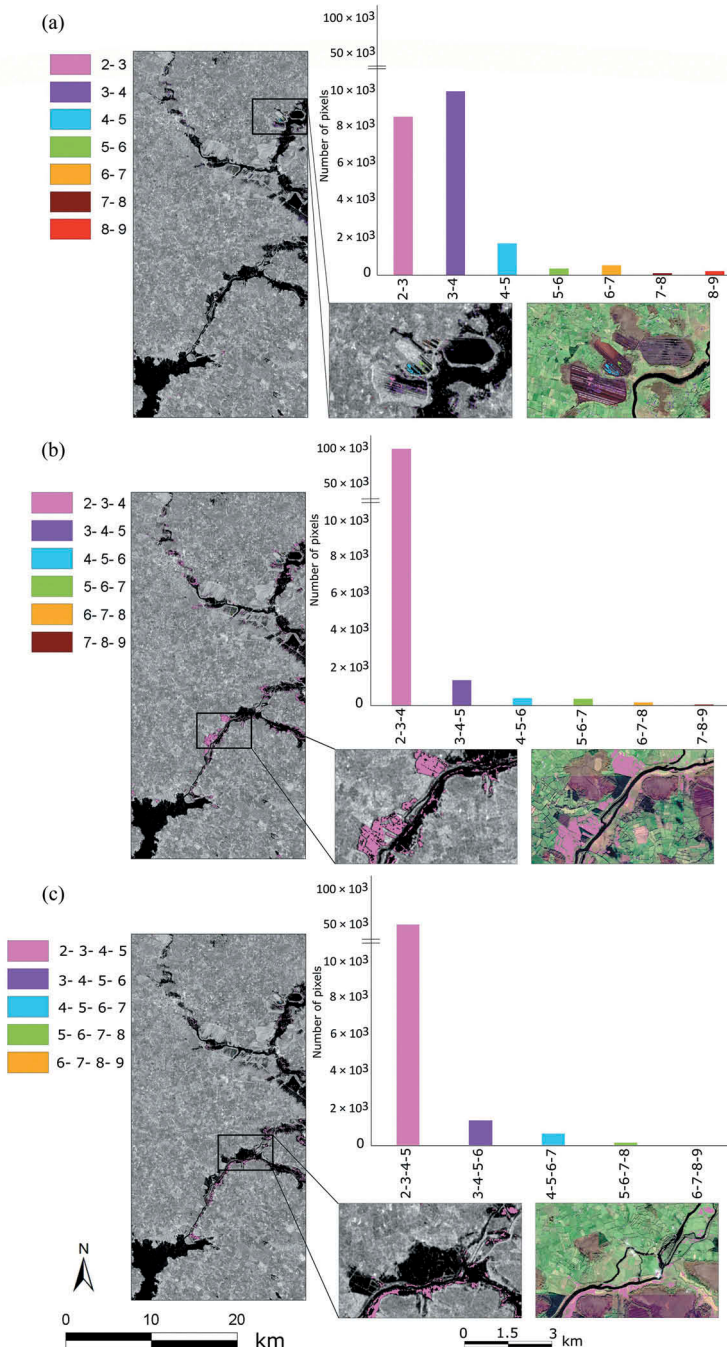


Figure 12. Distribution and mapping of temporary surface water surfaces' pixels classified (a) twice, (b) third or (c) fourth during the flood period (from t1 to t6, e.g., Figure 11) on the 09/01/16 Sentinel 1 image.

specifically designed for the properties of Sentinel-1 and Sentinel-2 data. Since these data are freely available, it is possible to analyse other flooding events in order to estimate statistically the proportion of land being regularly flooded which will be useful for flood risk management, especially for large catchments, region or nation-wide analyses. Considering the results, the proposed method could be established as a permanent service solution for global surface water mapping. However, it is important to extend the observation period, for example, to 5 years in order to be able to better understand surface water behaviour.

6. Conclusions and perspectives

A methodology for surface water detection by combining SAR (Sentinel-1) and optical (Sentinel-2) sensors is proposed using decision-level fusion rules. The methodology is applied over one hydrological year for the catchment of the Shannon river (Ireland) which has been severely impacted by flooding in Winter 2015/2016. The proposed methodology allows reducing the noise and increasing the detection level for time series of Sentinel-1 images, for multi-date Sentinel-2 images, and for the combination of both SAR and optical time series. Decision level rules are being tested for the particular case of surface water detection indicating that the Bayesian operator Sum is suitable for such application. Moreover, the analysis of image time series allows a better detection of both '*permanent surface water*' bodies (rivers and lakes) and '*temporary surface water*' bodies (flooded areas). It is further demonstrated that the fusion of SAR and optical time series increase the accuracy of the detection of the '*permanent surface water*' bodies. The proposed methodology is generic and does not require user interaction suggesting its application for monitoring '*permanent surface water*' bodies over large areas and at high temporal frequency, with the possibility of using it as a permanent service if integrated on high performance computing centre. For the monitoring of '*temporary surface water*' bodies, the use of decision-level rules allows quantifying the probability of occurrence of inundated terrains at the pixel scale giving the possibility to understand the space and time dynamics of the flooding. Such approach is of interest in improving flood risk management procedures.

Acknowledgements

This research is supported by the Indonesia Endowment Fund for Education (LPDP), Ministry of Finance, Republic of Indonesia and the French funded program ANR TIMES "*High-performance processing techniques for mapping and monitoring environmental changes from massive, heterogeneous and high frequency data times series*" (ANR-17-CE23-0015-01). It is a continuation of the research efforts carried out at LIVE and EOST on satellite image time series processing for the analysis of environmental processes. It is a contribution to the program A²S '*Satellite Surveillance Application*' of University of Strasbourg on the development of innovative processing chains for Sentinel data.

Author Contributions

Filsa Bioresita performed the experiments, collected and analysed the data, carried out some programming, and wrote the paper; Anne Puissant defined the research problem, proposed the



methodology, designed the experiments and contributed to the paper writing; André Stumpf and Jean-Philippe Malet gave useful advice, and contributed to the paper writing.

Disclosure statement

No potential conflict of interest was reported by the authors.

Funding

This work was supported by the Indonesia Endowment Fund for Education (LPDP), Ministry of Finance, Republic of Indonesia and the French funded program ANR-17-CE23-0015.

References

- Bartsch, A., A. M. Trofaier, G. Hayman, D. Sabel, S. Schlaffer, D. B. Clark, and E. Blyth. 2012. "Detection of Open Water Dynamics with Envisat ASAR in Support of Land Surface Modelling at High Latitudes." *Biogeosciences* 9: 703–714. doi:[10.5194/bg-9-703-2012](https://doi.org/10.5194/bg-9-703-2012).
- Benaglia, T., D. Chauveau, D. Hunter, and D. Young. 2009. "Mixtools: An R Package for Analyzing Finite Mixture Models." *Journal of Statistical Software* 32: 1–29. doi:[10.18637/jss.v032.i06](https://doi.org/10.18637/jss.v032.i06).
- Benediktsson, J. A., G. Cavallaro, N. Falco, I. Hedhli, V. A. Krylov, G. Moser, S. B. Serpico, and J. Zerubia. 2018. "Remote Sensing Data Fusion: Markov Models and Mathematical Morphology for Multisensor, Multiresolution, and Multiscale Image Classification." *Mathematical Models Remote Sensing Image Process* 277–323. doi:[10.1007/978-3-319-66330-2_7](https://doi.org/10.1007/978-3-319-66330-2_7).
- Bioresita, F., A. Puissant, A. Stumpf, and J.-P. Malet. 2018. "A Method for Automatic and Rapid Mapping of Water Surfaces from Sentinel-1 Imagery." *Remote Sensing* 10: 217. doi:[10.3390/rs10020217](https://doi.org/10.3390/rs10020217).
- Bourgeau-Chavez, L. L., K. Riordan, R. B. Powell, N. Miller, and M. Nowels. 2009. "Improving Wetland Characterization with Multi-Sensor, Multi-Temporal SAR and Optical/Infrared Data Fusion." *Advanced Geoscience and Remote Sensing*. doi:[10.5772/8327](https://doi.org/10.5772/8327).
- Chaouch, N., M. Temimi, S. Hagen, J. Weishampel, S. Medeiros, and R. Khanbilvardi. 2012. "A Synergetic Use of Satellite Imagery from SAR and Optical Sensors to Improve Coastal Flood Mapping in the Gulf of Mexico: Flood Mapping in the Gulf of Mexico Using Satellite Imagery." *Hydrological Processes* 26: 1617–1628. doi:[10.1002/hyp.v26.11](https://doi.org/10.1002/hyp.v26.11).
- Chavez, P. S. 1991. "Comparison of Three Different Methods to Merge Multiresolution and Multispectral Data: LandsatTM and SPOT Panchromatic." *Photogrammetric Engineering*, 57: 9.
- Chengquan, H., B. DeVries, H. Wenli, H. Lang, M. W. Jones, J. W., and F. Irena. 2018. Synergies of Landsat, Sentinel-2, and -1 for improved characterization of surface water dynamics. MWBS, Mapping Water Bodies from Space 2nd Conference, 27–28 March 2018, Frascati (Rome), Italy.
- Clement, M. A., C. G. Kilsby, and P. Moore. 2017. "Multi-Temporal Synthetic Aperture Radar Flood Mapping Using Change Detection: Multi-Temporal SAR Flood Mapping Using Change Detection." *Journal of Flood Risk Management*. doi:[10.1111/jfr3.12303](https://doi.org/10.1111/jfr3.12303).
- Copernicus. 2015a. "Water and Wetness Probability Index 2015." Copernic. Land Monit. Syst. Water Wetness Probab. Index 2015. Accessed March 5 18. <https://land.copernicus.eu/pan-european/high-resolution-layers/water-wetness/expert-products/wetness-probability-index/2015/view>
- Copernicus. 2015b. "Copernicus Emergency Management Service - Mapping." *Copernicus Emergency Management Service - Mapp*. Accessed 26 August 16.
- DeVries, B., C. Huang, M. Lang, J. Jones, W. Huang, I. Creed, M. Carroll, et al. 2017. "Automated Quantification of Surface Water Inundation in Wetlands Using Optical Satellite Imagery." *Remote Sens* 9: 807. doi:[10.3390/rs9080807](https://doi.org/10.3390/rs9080807).

- Du, Y., Y. Zhang, F. Ling, Q. Wang, W. Li, and X. Li. 2016. "Water Bodies' Mapping from Sentinel-2 Imagery with Modified Normalized Difference Water Index at 10-M Spatial Resolution Produced by Sharpening the SWIR Band." *Remote Sensing* 8, 354. doi:[10.3390/rs8040354](https://doi.org/10.3390/rs8040354).
- Éireann, M. 2015. "Record Breaking Rainfall and Temperature in Places." *Monthly Weather Bulletin* 355: 1–2. <http://edepositireland.ie/bitstream/handle/2262/77494/clim-2015-Dec.pdf?sequence=1&isAllowed=y>.
- Éireann, M., 2016. "Met Éireann The Irish Meteorological Service." Available Data - Met ÉireannThe Ir. Meteorological Serv. Accessed 26 August 16.<https://www.met.ie/climate/available-data>
- Epa, I., 2017. "EPA Ireland Catalogue - Geo Portal." EPA Irel. Cat. - EPA Irel. URL. Accessed 23 October 18. <https://gis.epa.ie/geonetwork/srv/eng/catalog.search#/home>
- EROS Center, 2018. "Collection-1 Landsat Level-3 Dynamic Surface Water Extent (DWSE) Science Product." doi:[10.5066/F7445KQK](https://doi.org/10.5066/F7445KQK).
- Farr, T. G., P. A. Rosen, E. Caro, R. Crippen, R. Duren, S. Hensley, M. Kobrick, et al. 2007. "The Shuttle Radar Topography Mission." *Reviews of Geophysics* 45. doi:[10.1029/2005RG000183](https://doi.org/10.1029/2005RG000183).
- Feyisa, G. L., H. Meilby, R. Fensholt, and S. R. Proud. 2014. "Automated Water Extraction Index: A New Technique for Surface Water Mapping Using Landsat Imagery." *Remote Sensing of Environment* 140: 23–35. doi:[10.1016/j.rse.2013.08.029](https://doi.org/10.1016/j.rse.2013.08.029).
- Foumelis, M., 2015. "ESA Sentinel-1 Toolbox Generation of SAR Backscattering Mosaics, Course Materials." In 6th ESA Advanced Training Course on Land Remote Sensing, 14–18 September 2015, Bucharest, Romania.
- Freeman, J. B., and R. Dale. 2013. "Assessing Bimodality to Detect the Presence of a Dual Cognitive Process." *Behavior Research Methods* 45: 83–97. doi:[10.3758/s13428-012-0225-x](https://doi.org/10.3758/s13428-012-0225-x).
- Gamba, P. 2014. "Image and Data Fusion in Remote Sensing of Urban Areas: Status Issues and Research Trends." *International Journal of Image and Data Fusion* 5: 2–12. doi:[10.1080/19479832.2013.848477](https://doi.org/10.1080/19479832.2013.848477).
- Ghassemian, H. 2016. "A Review of Remote Sensing Image Fusion Methods." *Information Fusion* 32: 75–89. doi:[10.1016/j.inffus.2016.03.003](https://doi.org/10.1016/j.inffus.2016.03.003).
- Goyal, S., and R. Wahla. 2015. "A Review on Image Fusion." *International Journal of Innovative Research in Computer and Communication Engineering* 3: 7582–7588. doi:[10.15680/IJRCCE.2015.0308104](https://doi.org/10.15680/IJRCCE.2015.0308104).
- Huang, W., B. DeVries, C. Huang, M. Lang, J. Jones, I. Creed, and M. Carroll. 2018. "Automated Extraction of Surface Water Extent from Sentinel-1 Data." *Remote Sens*, no. 10: 797. doi:[10.3390/rs10050797](https://doi.org/10.3390/rs10050797).
- Jiang, H., M. Feng, Y. Zhu, N. Lu, J. Huang, and T. Xiao. 2014. "An Automated Method for Extracting Rivers and Lakes from Landsat Imagery." *Remote Sensing* 6: 5067–5089. doi:[10.3390/rs6065067](https://doi.org/10.3390/rs6065067).
- Joshi, N., M. Baumann, A. Ehammer, R. Fensholt, K. Grogan, P. Hostert, M. R. Jepsen, et al. 2016. "A Review of the Application of Optical and Radar Remote Sensing Data Fusion to Land Use Mapping and Monitoring." *Remote Sensing* 8: 70. doi:[10.3390/rs8010070](https://doi.org/10.3390/rs8010070).
- Langanke, T. 2016. *Copernicus Land Monitoring Service – High Resolution Layer Water and Wetness Product Specifications Document*. Copernicus - European Environment Agency - European Commission.
- Lehner, B., and P. Döll. 2004. "Development and Validation of a Global Database of Lakes, Reservoirs and Wetlands." *Journal of Hydrology* 296: 1–22. doi:[10.1016/j.jhydrol.2004.03.028](https://doi.org/10.1016/j.jhydrol.2004.03.028).
- Liu, Z., E. Blasch, G. Bhatnagar, V. John, W. Wu, and R. S. Blum. 2018. "Fusing Synergistic Information from Multi-Sensor Images: An Overview from Implementation to Performance Assessment." *Information Fusion* 42: 127–145. doi:[10.1016/j.inffus.2017.10.010](https://doi.org/10.1016/j.inffus.2017.10.010).
- Louis, J., V. Debaecker, B. Pflug, M. Main-Knorn, J. Bieniarz, U. Mueller-Wilm, E. Cadau, and F. Gascon, 2016. "Sentinel-2 Sen2cor: L2a Processor for Users." In Proceedings of the Living Planet Symposium. Presented at the ESA Living Planet Symposium, Prague, Czech Republic, p. 8.
- Marcus, W. A., and M. A. Fonstad. 2008. "Optical Remote Mapping of Rivers at Sub-Meter Resolutions and Watershed Extents." *Earth Surface Processes and Landforms* 33: 4–24. doi:[10.1002/\(ISSN\)1096-9837](https://doi.org/10.1002/(ISSN)1096-9837).

- Markert, K. N., F. Chishtie, E. R. Anderson, D. Saah, and R. E. Griffin. 2018. "On the Merging of Optical and SAR Satellite Imagery for Surface Water Mapping Applications." *Results in Physics* 9: 275–277. doi:[10.1016/j.rinp.2018.02.054](https://doi.org/10.1016/j.rinp.2018.02.054).
- Martinis, S. 2010. "Automatic Near Real-time Flood Detection in High Resolution X-Band Synthetic Aperture Radar Satellite Data Using Context-Based Classification on Irregular Graphs." PhD thesis, Fakultät für Geowissenschaften, Ludwig-Maximilians-Universität München, Germany.
- Martinis, S., 2017. "Improving Flood Mapping in Arid Areas Using Sentinel-1 Time Series Data." In *2017 IEEE International Geoscience Proceeding*, 193–196. Fort Worth, TX.
- Martinis, S., and A. Twele. 2010. "A Hierarchical Spatio-Temporal Markov Model for Improved Flood Mapping Using Multi-Temporal X-Band SAR Data." *Remote Sensing* 2: 2240–2258. doi:[10.3390/rs2092240](https://doi.org/10.3390/rs2092240).
- Martinis, S., A. Twele, and S. Voigt. 2009. "Towards Operational near Real-Time Flood Detection Using a Split-Based Automatic Thresholding Procedure on High Resolution TerraSAR-X Data." *Natural Hazards and Earth System Sciences* 9: 303–314. doi:[10.5194/nhess-9-303-2009](https://doi.org/10.5194/nhess-9-303-2009).
- Matgen, P., M. Montanari, R. Hostache, L. Pfister, L. Hoffmann, D. Plaza, V. R. N. Pauwels, G. J. M. De Lannoy, R. De Keyser, and H. H. G. Savenije. 2010. "Towards the Sequential Assimilation of SAR-derived Water Stages into Hydraulic Models Using the Particle Filter: Proof of Concept." *Hydrology and Earth System Sciences* 14: 1773–1785. doi:[10.5194/hess-14-1773-2010](https://doi.org/10.5194/hess-14-1773-2010).
- McCarthy, M., S. Spillane, S. Walsh, and M. Kendon. 2016. "The Meteorology of the Exceptional Winter of 2015/2016 across the UK and Ireland." *Weather* 71: 305–313. doi:[10.1002/wea.2016.71.issue-12](https://doi.org/10.1002/wea.2016.71.issue-12).
- McFeeters, S. K. 1996. "The Use of the Normalized Difference Water Index (NDWI) in the Delineation of Open Water Features." *International Journal of Remote Sensing* 17: 1425–1432. doi:[10.1080/01431169608948714](https://doi.org/10.1080/01431169608948714).
- Muster, S., B. Heim, A. Abnizova, and J. Boike. 2013. "Water Body Distributions across Scales: A Remote Sensing Based Comparison of Three Arctic Tundra Wetlands." *Remote Sensing* 5: 1498–1523. doi:[10.3390/rs5041498](https://doi.org/10.3390/rs5041498).
- Nath, R. K., and S. K. Deb. 2010. "Water-Body Area Extraction from High Resolution Satellite Images-An Introduction, Review, and Comparison." *International Journal of Image Processing* 3: 353–372.
- National Directorate for Fire and Emergency Management. 2016. *Report on Flooding December 4 2015 – January 13 2016*. Ireland: Department of Housing, Planning, Community and Local Government.
- Nga, N. G.-I. A. 2005. *Documentation for the Shuttle Radar Topography Mission (SRTM) Water Body Data Files*. USGS.
- Ogashawara, I., D. R. Mishra, and A. A. Gitelson. 2017. "Remote Sensing of Inland Waters, In: Bio-Optical Modeling and Remote Sensing of Inland Waters." Elsevier 1–24. doi:[10.1016/B978-0-12-804644-9.00001-X](https://doi.org/10.1016/B978-0-12-804644-9.00001-X).
- Ogilvie, A., G. Belaud, S. Massuel, M. Mulligan, P. Le Gouven, and R. Calvez. 2018. "Surface Water Monitoring in Small Water Bodies: Potential and Limits of Multi-Sensor Landsat Time Series." *Hydrology and Earth System Sciences* 1–35. doi:[10.5194/hess-2018-19](https://doi.org/10.5194/hess-2018-19).
- Pappenberger, F., K. Frodsham, K. Beven, R. Romanowicz, and P. Matgen. 2007. "Fuzzy Set Approach to Calibrating Distributed Flood Inundation Models Using Remote Sensing Observations." *Hydrology and Earth System Sciences* 11: 739–752.
- Pekel, J.-F., A. Cottam, N. Gorelick, and A. S. Belward. 2016. "High-Resolution Mapping of Global Surface Water and Its Long-Term Changes." *Nature* 540: 418. doi:[10.1038/nature20584](https://doi.org/10.1038/nature20584).
- Pierdicca, N., L. Pulvirenti, M. Chini, L. Guerriero, and L. Candela. 2013. "Observing Floods from Space: Experience Gained from COSMO-SkyMed Observations." *Acta Astronautica* 84: 122–133. doi:[10.1016/j.actaastro.2012.10.034](https://doi.org/10.1016/j.actaastro.2012.10.034).
- Pohl, C., and J. L. Van Genderen. 1998. "Review Article Multisensor Image Fusion in Remote Sensing: Concepts, Methods and Applications." *International Journal of Remote Sensing* 19: 823–854. doi:[10.1080/014311698215748](https://doi.org/10.1080/014311698215748).
- Rennó, C. D., A. D. Nobre, L. A. Cuartas, J. V. Soares, M. G. Hodnett, J. Tomasella, and M. J. Waterloo. 2008. "HAND, a New Terrain Descriptor Using SRTM-DEM: Mapping Terra-Firme Rainforest

- Environments in Amazonia." *Remote Sensing of Environment* 112: 3469–3481. doi:[10.1016/j.rse.2008.03.018](https://doi.org/10.1016/j.rse.2008.03.018).
- Riffler, M., A. Moran, B. Dullek, C. Schleicher, A. Walli, and J. Weichselbaum. 2018. "Large-scale Water and Wetness Detection Using a Multi-sensor and Multi-temporal Approach." MWBS, Mapping Water Bodies from Space 2nd Conference, Frascati (Rome), Italy, March 27–28.
- Rokni, K., A. Ahmad, A. Selamat, and S. Hazini. 2014. "Water Feature Extraction and Change Detection Using Multitemporal Landsat Imagery." *Remote Sensing* 6: 4173–4189. doi:[10.3390/rs6054173](https://doi.org/10.3390/rs6054173).
- Schindler, K. 2012. "An Overview and Comparison of Smooth Labeling Methods for Land-Cover Classification." *IEEE Geoscience and Remote Sensing Magazine* 50: 4534–4545.
- Schmitt, M., and X. X. Zhu. 2016. "Data Fusion and Remote Sensing: An Ever-Growing Relationship." *IEEE Geoscience and Remote Sensing Magazine* 4: 6–23. doi:[10.1109/MGRS.2016.2561021](https://doi.org/10.1109/MGRS.2016.2561021).
- Schumann, G., G. Di Baldassarre, and P. D. Bates. 2009. "The Utility of Spaceborne Radar to Render Flood Inundation Maps Based on Multialgorithm Ensembles." *IEEE Geoscience and Remote Sensing Magazine* 47: 2801–2807. doi:[10.1109/TGRS.2009.2017937](https://doi.org/10.1109/TGRS.2009.2017937).
- Stewart, C., 2016. "Exercise Sentinel-1 Processing, Course Materials." In 8th ESA Training Course on Radar and Optical Remote Sensing, Cesis, Latvia, 5-9 September 2016.
- The European Commission's Joint Research Centre, 2016. "Global Surface Water - Data Access." Glob. Surf. Water - Data Access. Accessed June 3 18. <https://global-surface-water.appspot.com/download>
- Twele, A., W. Cao, S. Plank, and S. Martinis. 2016. "Sentinel-1-Based Flood Mapping: A Fully Automated Processing Chain." *International Journal of Remote Sensing* 37: 2990–3004. doi:[10.1080/01431161.2016.1192304](https://doi.org/10.1080/01431161.2016.1192304).
- Voigt, S., T. Kemper, T. Riedlinger, R. Kiefl, K. Scholte, and H. Mehl. 2007. "Satellite Image Analysis for Disaster and Crisis-Management Support." *IEEE Transactions on Geoscience and Remote Sensing* 45: 1520–1528. doi:[10.1109/TGRS.2007.895830](https://doi.org/10.1109/TGRS.2007.895830).
- Wang, Y., F. Huang, and Y. Wei, 2013. "Water Body Extraction from LANDSAT ETM+ Image Using MNDWI and K-T Transformation." In Presented at the Geoinformatics 2013 21st International Conference, Kaifeng, Henan, China: Henan University.
- Wendl, C., A. Le Bris, N. Chehata, A. Puissant, and T. Postadjian, 2018. "Decision Fusion of SPOT-6 and Multitemporal Sentinel-2 Images for Urban Area Detection." In Proceeding of The IEEE International Geoscience and Remote Sensing Symposium (IGARSS), Valencia, Spain: Presented at the IEEE International Geoscience and Remote Sensing Symposium (IGARSS).
- Westerhoff, R. S., M. P. H. Kleuskens, H. C. Winsemius, H. J. Huizinga, G. R. Brakenridge, and C. Bishop. 2013. "Automated Global Water Mapping Based on Wide-Swath Orbital Synthetic-Aperture Radar." *Hydrology and Earth System Sciences* 17: 651–663. doi:[10.5194/hess-17-651-2013](https://doi.org/10.5194/hess-17-651-2013).
- WWF. 2004. "Global Lakes and Wetlands Database." Glob. Lakes Wetl. Database. Accessed June 1 18. <https://www.worldwildlife.org/pages/global-lakes-and-wetlands-database>
- Zadeh, L. A. 1976. "A Fuzzy-Algorithmic Approach to the Definition of Complex or Imprecise Concepts." *System Theory Social Science Interdisciplinary System Research*.